Research Article

Tobias Ruess*, Gerd Gantenbein, Zisis Ioannidis, Tomasz Rzesnicki, Dietmar Wagner, Manfred Thumm, and John Jelonnek

Frequency and Mode Measurement Techniques for Megawatt-class Gyrotrons

https://doi.org/10.1515/sample-YYYY-XXXX
Received Month DD, YYYY; revised Month DD, YYYY; accepted Month DD, YYYY

Abstract: State-of-the-art vacuum electron tubes such as gyrotrons, deliver RF output powers up to more than 2 MW at frequencies up to 170 GHz. In terms of the very high power levels, a proper verification of the gyrotron components itself and measurements during gyrotron operation are vital to prevent possible fatal errors. Several basic RF measurement setups, which are used at IHM/KIT, are discussed. Currently, their upper frequency limit is 175 GHz. In terms of future gyrotron operation above 200 GHz, upgrades of the measurement setups for operation up to 260-330 GHz are prepared. The experimental devices discussed herein are a quasi-optical mode generator for the verification of the quasi-optical gyrotron output system, the window measurement test stand to verify the ceramic gyrotron output window and the frequency diagnostic system to measure the operating frequency and thereby the excited mode.

Keywords: gyrotron, RF measurement setup, mode generator, high-order modes, RF windows, frequency diagnostic

1 Introduction

A gyrotron is a vacuum electron tube providing RF output power in the MW-range at frequencies above 100 GHz. A sketch and a photo of the KIT 170 GHz 2 MW $TE_{34,19}$-mode coaxial-cavity modular short-pulse pre-prototype is shown in Fig. 1. In principle, a gyrotron is an oscillator which is based on the interaction of a weakly relativistic electron beam and a transverse electric cavity mode $TE_{m,p}$. The electron beam is generated by a Magnetron Injection Gun. The emitted electrons are accelerated by the applied voltages and are guided by the magnetic field lines of the super-conducting magnet. The operating frequency is dependent on the applied maximum magnet field strength. Oversized waveguides are chosen for the cavity, where high-order modes are excited to reduce the cavity wall loading. The generated RF beam is coupled out of the gyrotron using a quasi-optical output system. The energy of the spent electron beam is dissipated in the collector.

Megawatt-class gyrotrons are mainly applied in fusion plasma machines for Electron Cyclotron Resonance Heating and Current Drive (ECRH&CD) [3] and plasma stabilization [4]. Two large plasma experiments are located in Germany, namely ASDEX Upgrade [5] in Garching and Wendelstein 7-X [6] in Greifswald. The stellarator Wendelstein 7-X is equipped with ten continuous wave (CW) gyrotrons, each producing 1 MW RF output power at 140 GHz. The ECRH&CD system at ASDEX Upgrade employs 8 two-frequency 1 MW gyrotrons with 10 s pulse length, operating at 105 GHz or 140 GHz. Current project under construction is the international tokamak ITER in Caderache, France [7]. This fusion machine will be equipped with up to 24 gyrotrons operating at 170 GHz and delivering 1 MW CW RF output power per tube. ITER

***Corresponding author: Tobias Ruess,** Karlsruhe Institute of Technology, Institute of Radio Frequency Engineering and Electronics (IHE) and Institute for Pulsed Power and Microwave Technology (IHM), Karlsruhe, Germany, e-mail: tobias.ruess@kit.edu
Gerd Gantenbein, Zisis Ioannidis, Tomasz Rzesnicki, Manfred Thumm, John Jelonnek, Karlsruhe Institute of Technology, Institute for Pulsed Power and Microwave Technology, Karlsruhe, Germany
Dietmar Wagner, Max-Planck-Institute for Plasma Physics, IPP Garching, Germany

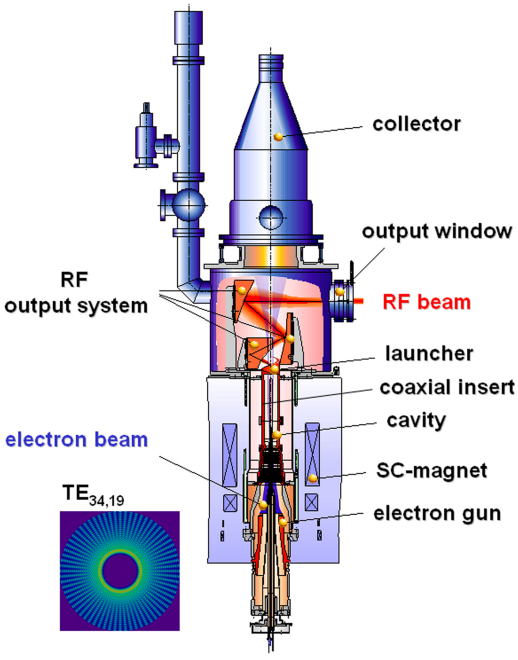

(a) Sketch of the KIT 170 GHz 2 MW $TE_{34,19}$-mode coaxial-cavity modular short-pulse pre-prototype.

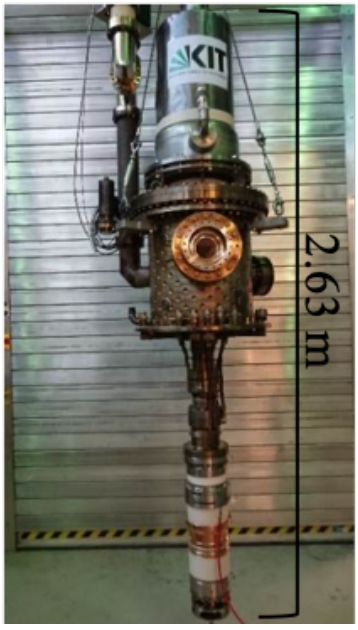

(b) Photo of the KIT 170 GHz 2 MW $TE_{34,19}$-mode coaxial-cavity modular short-pulse pre-prototype.

Fig. 1: Sketch [1] and photo [2] of the KIT 170 GHz 2 MW $TE_{34,19}$-mode coaxial-cavity modular short-pulse pre-prototype gyrotron.

is a scientific project to demonstrate the suitability of the tokamak concept and will be the basis for a Demonstration Fusion Power Plant (DEMO) [8]. The European DEMO baselines foresee multi-frequency and multi-purpose gyrotrons operating at 170/204 GHz and probably 136 GHz in future, with a frequency step-tunability of ± 10 GHz in 2-3 GHz steps around each center frequency. The RF output power is defined by 2 MW per tube.

For R&D of the required DEMO gyrotrons, the IHM/KIT is constructing a Fusion Long Pulse Gyrotron Laboratory (FULGOR) [9], which is equipped with a 10 MW CW high-voltage power supply and a 10.5 T super-conducting magnet. The first gyrotron experiments are planned to be done in 2022. The FULGOR test facility exceeds the current gyrotron frequency limitation of 170 GHz. In terms of the current limited operating frequency, all available measurement systems are also limited to 175 GHz. Therefore, the existing measurement setups are upgraded towards an operation up to 330 GHz, which is the limit of the available frequency extension modules at IHM/KIT.

The measurement devices used for the gyrotron verification can be separated into two categories. The first includes low power measurement systems that are used to validate gyrotron key components before installation into the gyrotron. Those measurement systems are the mode generator for the validation of the quasi-optical gyrotron output system and the test stand for measuring the transparency and/or reflection of the gyrotron ceramic output window. These setups are operating in the low power regime where no electron beam, super-conducting magnet and high-voltage power supply are required ("cold measurements"). Nevertheless, these measurements are vital because the components do not allow any design failures and accept manufacturing tolerances of only few micrometers for proper operation. These setups excite the desired input modes (e.g. the transverse electric $TE_{m,p}$ gyrotron cavity mode and the linearly polarized fundamental Gaussian output mode) to verify the given gyrotron component. The second category of measurement systems is used for the validation of the gyrotron operation ("hot measurements"). Examples for this category are the frequency diagnostic system and the power measurement equipment [10]. This paper focuses only on the frequency dependent parts of the measurement setups. Therefore, the power

measurement is not discussed further. The frequency diagnostic system records the operating frequency of the gyrotron where e.g. mode stability, mode jumps and parasitic RF oscillations can be detected.

In the following, the basic principle of each measurement setup is presented and the relevant upgrades that are required to verify the gyrotron performance are discussed.

2 Verification of the Quasi-Optical Output System

In a fusion device, the RF power generated by the gyrotron has to be transmitted from the gyrotron location to the plasma vessel. Typical lengths of the transmission lines range from 40 m to more than 100 m. The millimeter (mm)-waves are guided by waveguides or quasi-optical transmission lines either evacuated or under atmospheric pressure. The high-order rotating $TE_{m,p}$ gyrotron cavity modes, like the $TE_{28,10}$ mode [11], suffer from high transmission losses. Therefore, a mode conversion of the gyrotron mode is required. The so-called quasi-optical (q.-o.) output system, consisting of a specific waveguide antenna (launcher) and several mirrors, converts the operating cavity mode into a linearly polarized fundamental Gaussian-beam. The q.-o. output system does not allow any design failures and accept manufacturing tolerances of only a few micrometers for a proper operation. Therefore, low power tests of these key gyrotron components are vital before the installation into the gyrotron. For a proper verification of the q.-o. output system, the operating high-order cavity mode has to be excited in a circular waveguide cavity with a geometry similar to the high-power gyrotron cavity at low power, without a gyrotron. The excited gyrotron mode has to be provided at the input of the q.-o. output system. Such a rotating high-order mode in the low power regime can be excited using a so-called quasi-optical mode generator [12].

2.1 Quasi-Optical Mode Generator Setup

The setup of a quasi-optical mode generator can be seen in Fig. 2a. The device consists of a rectangular-to-circular waveguide transition and a step-tapered horn antenna to transform the $TE_{1,0}$ mode from the rectangular mono-mode waveguide to a Gaussian-beam, TEM_{00} mode, which is launched as a spherical wave to Teflon lenses. The Teflon lenses produce an astigmatic Gaussian-like beam (TEM_{00} mode) which is focused onto a quasi-parabolic (q.-p.) mirror, where the astigmatism helps to reduce spillover losses. The q.-p. mirror can be adjusted by linear drivers. The focused beam couples through the thin cavity wall, which is perforated with small cutoff-holes and excites the resonant cavity mode. The cavity is specially designed for the low-power tests using a scattering matrix code [13]. An additional non-linear up-taper is assembled to the mode generator cavity, as can be seen in Fig. 2b, to increase the spatial resolution of the measurement. The field pattern is measured at the end of the non-linear up-taper using a rectangular standard waveguide pick-up antenna, which is mounted on a 3D measurement arm. The received signal is evaluated using a vector network analyzer (VNA) of the PNA series.

2.2 Measurements of High-Order Modes

In highly oversized circular waveguides, besides the fundamental mode, a large number of eigenmodes can propagate. In general, N modes can be excited, where $N \approx 2.55 \cdot \left(\frac{2R}{\lambda_0}\right)$ with the waveguide radius R and λ_0 the free-space wavelength. This implies, that more than 1000 modes could be excited in cavities used for MW-class gyrotrons. The number of propagating modes increases with increasing frequency. Therefore, a precise adjustment of the q.-p. mirror of the mode generator setup is mandatory for a correct excitation with high mode purity at very high frequencies. At IHM/KIT, the q.-p. mirror adjustment has been upgraded from the manual adjustment to computer-controlled high-precision linear drivers. Starting from this point, all relevant components of the measurement are controlled by a PC, which was the start of an automated

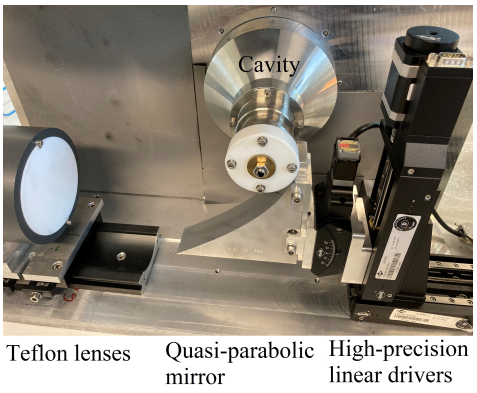

(a) Main components of mode generator setup. An astigmatic Gaussian-like beam is formed by the horn antenna and the Teflon lenses. This beam is focused on the perforated wall of the cavity using a quasi-parabolic mirror.

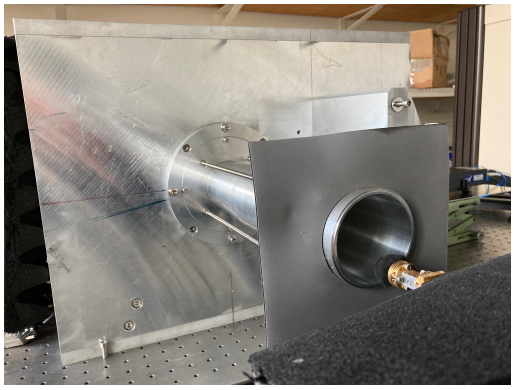

(b) Mode generator setup with assembled non-linear up-taper. The measurement plane is at the end of the non-linear up-taper.

Fig. 2: Photos of the quasi-optical mode generator setup.

mode generator process. The flow chart of the automated measurement procedure is presented in [14]. The current system can evaluate the azimuthal m and radial p mode index, the operating frequency, the quality factor of the cavity and the scalar mode content. The modified test stand can operate from 90-330 GHz using three different frequency extension modules working in the frequency ranges from 90-140, 140-220 and 220-330 GHz.

A measurement of the $TE_{40,23}$ mode pattern at 204.074 GHz is shown in amplitude and phase in Fig. 3. Its radial mode index can be determined by the number of rings ($p = 23$) and the azimuthal mode index of the number of phase jumps plus one ($m = 40$). The calculated scalar mode content is higher than 92 % with a counter-rotating amount of 0.8 %. Only one polarization can be measured in terms of using a standard pick-up antenna as the receiving antenna. Therefore, the measurement is performed in Cartesian coordinates instead of Polar. This can be expressed by a coordinate transformation and results in:

$$E_x = E_r \cdot \cos(\varphi) - E_\varphi \cdot \sin(\varphi), \tag{1}$$

$$E_y = E_r \cdot \sin(\varphi) + E_\varphi \cdot \cos(\varphi), \tag{2}$$

where $E_r \sim J_m(\frac{\chi_{m,p} \cdot r}{R})$ and $E_\varphi \sim J'_m(\frac{\chi_{m,p} \cdot r}{R})$. In Fig. 3, the measurement of the y-polarization of a mode is shown. Regarding $\varphi = 0°$ and $\varphi = 180°$ the first term of E_y is zero, where only the field component

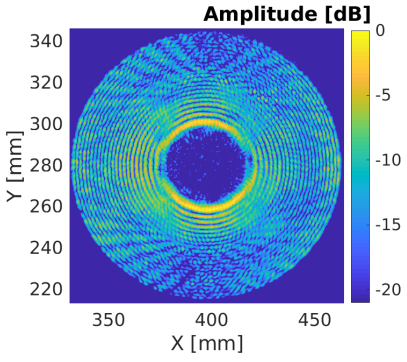

(a) Field intensity pattern.

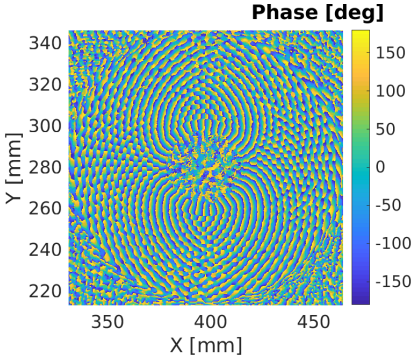

(b) Phase pattern.

Fig. 3: Field intensity and phase pattern of $TE_{40,23}$ mode at 204.074 GHz of the E_y polarization.

in φ-direction can be measured and in $\varphi = 90°$ and $\varphi = 270°$ the second term is zero. This concludes that there is a $J'_m(\frac{\chi_{m,p} \cdot r}{R})$ dependency in $\varphi = 0°$ and $\varphi = 180°$ direction and a $J_m(\frac{\chi_{m,p} \cdot r}{R})$ dependency in $\varphi = 90°$ and $\varphi = 270°$ direction, following that the graph is not rotational symmetric. The full mode pattern can be calculated if both polarization are measured separately. However, for component validation this calculation is not required.

2.3 Verification of the Quasi-Optical Output System

The successfully excited mode is used for the verification of the quasi-optical output system. In this measurement, the mode generator setup is rotated by 90° and the non-linear up-taper is replaced by the launcher and mirrors. A verification of the q.-o. output system of the $TE_{28,10}$ mode at 140.006 GHz [11] using a similar mode generator setup with a correspondingly modified cavity is shown in Fig. 4. The amplitude and phase are measured using a VNA. The measurement results are presented in Fig. 5, where the measurement plane is in a distance of 350 mm to the gyrotron axis, according to Fig. 1. The calculated vectorial mode content (amplitude and phase are considered) is calculated to be higher than 97 % using the mode matching method, which is integrated in TWLDO [15]. The calculated Gaussian mode content is in very good agreement with the simulations.

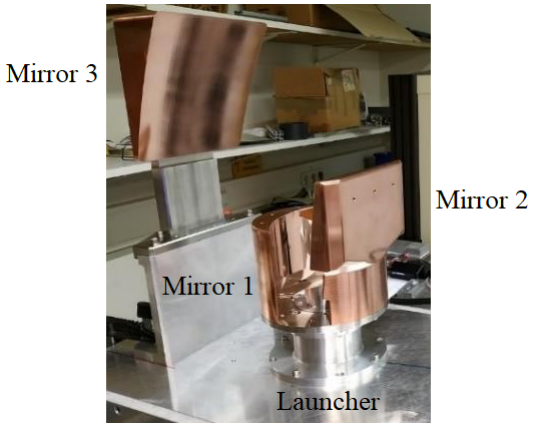

Fig. 4: Photo of the quasi-optical output system with launcher and three mirrors for the $TE_{28,10}$ mode at 140 GHz [11].

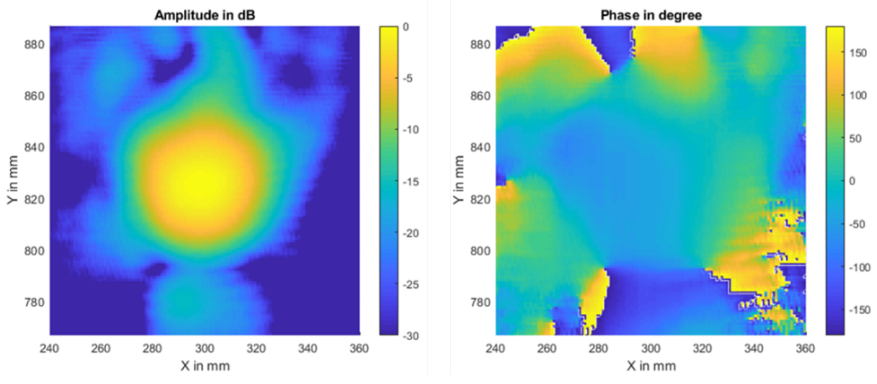

Fig. 5: Measured amplitude (left) and phase (right) of the quasi-optical output system for the $TE_{28,10}$ mode at 140 GHz [11] in a distance of 350 mm to the gyrotron axis.

3 Quasi-Optical Measurement on Gyrotron Output Windows

A highly transparent window is required to couple the mm-wave output beam converted by the q.-o. output system out of the evacuated gyrotron into free space. There are different possible window materials, which are summarized with their specifications in Tab. 1. Important material parameters are the failure resistance R' defined by the Youngs' Modulus E and the thermal expansion α to $R' \sim k/E\alpha$ and the RF-power transmission capacity defined by $P_T = \frac{R' \cdot \rho \cdot c_p}{(1+\epsilon_r') \tan\delta}$ [16], where ρ is the density, c_p is the specific heat capacity, ϵ_r' the relative permittivity and the loss tangent $\tan\delta$. BeO and SiC are in terms of low RF-power transmission capacity not suitable for long pulse operation. In contrast, Silicon and Diamond show a good RF performance. However, the thermal conductivity of Silicon is too low to be a candidate for windows in long pulse gyrotrons. Therefore, chemical-vapor deposition (CVD) diamond is used for long-pulse megawatt-class gyrotrons due to its best properties for this application. However, CVD-diamond is the most expensive material discussed. CVD-diamond has a relative permittivity of $\epsilon_r' = 5.67$, a very low loss tangent of $\approx 2 \cdot 10^{-5}$ and a very high thermal conductivity which allows the application of edge cooling technology.

Tab. 1: Summary of ceramic gyrotron output window materials and its properties [16].

Material	BeO	Silicon	SiC	CVD-Diamond
Thermal conductivity k [W/mK]	260	150	330	2000
Failure resistance R' $\left[\frac{\mathrm{W}}{\mathrm{mm}}\right]$	10.3	284	40	772
RF-power transmission capacity $P_T = \frac{R' \cdot \rho \cdot c_p}{(1+\epsilon_r') \tan\delta}$	0.06	106	0.63	106
Cost	medium	low	medium	very high

A gyrotron window is almost transparent at specific frequencies, only. These specific frequencies are the so-called natural resonances, given by [17]

$$f_{op} = n \cdot \frac{\lambda_M}{2} = \frac{n \cdot c_0}{2 \cdot d_{\mathrm{window}} \cdot \sqrt{\epsilon_r'}} \,. \tag{3}$$

A natural resonance occurs when the thickness d_{window} is a multiple n of half a wavelength in the medium λ_M.

3.1 Measurement Setup

A low-power measurement of the gyrotron window is performed before the installation into the gyrotron. This measurement setup has been upgraded using a VNA and extension modules covering the frequency band from 90-220 GHz. There are two possible methods for the verification of the gyrotron window, namely measuring the transmission or the reflection. A reflection measurement is a more compact setup, but no statement regarding absorption can be made. The operating gyrotron frequency should fit as best as possible to the natural resonance of the gyrotron output window because the reflected signal is guided towards the cavity and influences the interaction mechanism. Therefore, in the following the measurement setup for the determination of the reflection is discussed.

A schematic view of the reflection measurement is shown in Fig. 6a. The mm-waves are launched using a corrugated horn antenna. The wave is focused on the gyrotron window using two mirrors. In terms of measuring the reflection, the transmitting (Tx) and receiving (Rx) signal have to be separated. For this reason, a Mylar foil is used at a 45° angle for dividing the mm-wave. The incident wave on the Mylar foil in the Tx path is split into a reflected wave, which is attenuated by an absorber, and the transmitted wave, which is propagated to the gyrotron window. In the Rx path, the wave transmitted through the Mylar

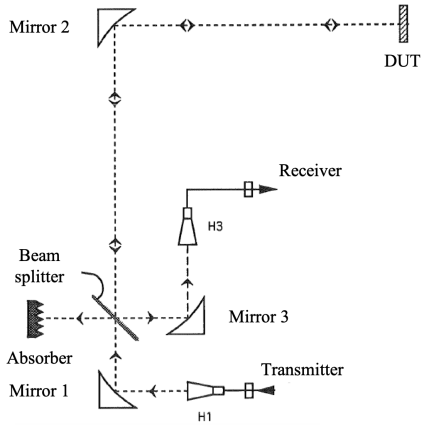

(a) Schematic of window measurement test stand.

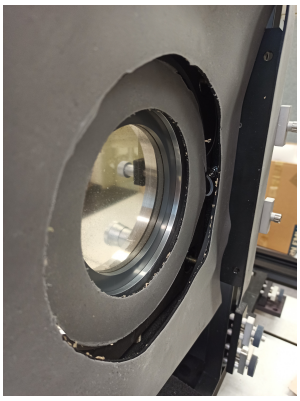

(b) Assembly of CVD-diamond window, where the metallic parts are covered by microwave absorber.

Fig. 6: Measurement setup for the verification of ceramic gyrotron window disks.

foil is forwarded to the transmitter. Therefore, an isolator is assembled between the extension module and the corrugated horn antenna to attenuate these field components. The reflected wave in the Rx path is focused with a third mirror to the corrugated receiving horn antenna. The evaluation of the measurement is performed using a VNA. A photo of the assembled CVD-disk is shown in Fig. 6b.

3.2 Measurement Results on a CVD-Diamond Output Window

A key aspect of the reflection measurement is a proper calibration. Only the amplitude information is important for this verification, which simplifies the calibration. Theoretically, a calibration with a highly conducting metal plate as reference measurement would be sufficient. However, multi-reflection reduces the quality of the measurements. Therefore, time gating is applied to eliminate the multi-reflection path. The propagation length between the transmitter and the gyrotron window is 1.5 m in one way, which allows the multi-reflections to be cut off with the correct span parameters. A span of $\pm$ 10 ns around the gate center, which corresponds to $\approx$ 3 m in free space, is applied. Both calibration methods are combined and result in a satisfactory calibration of the VNA.

In Fig. 7, a result of the verification of a CVD-disk is shown. The resonance frequency is determined to be 139.746 $\pm$ 0.02 GHz ($4 \cdot \lambda_M/2$) and 174.662 $\pm$ 0.05 GHz ($5 \cdot \lambda_M/2$). From this, the window thickness of 1.8019 $\pm$ 0.0005 mm has been calculated using Eq. 3 and the nominal relative permittivity. The measurement result is in good agreement with the thickness retrieved from mechanical measurements.

4 Frequency Diagnostic Measurements on Megawatt-class Gyrotrons

In this section, a frequency diagnostic system is discussed for the verification of the gyrotron operation. Each operating gyrotron mode has a specific operating frequency. Therefore, the operating frequency gives an indication of the operating mode in the gyrotron. Two different frequency diagnostic systems have been developed at IHM/KIT, namely the Frequency Measurement System (FMS) [18] and Pulse Spectrum Analyzer (PSA) [19]. The requirements for a frequency diagnostic system for the gyrotron operation are high dynamic range, frequency bandwidth of up to 18 GHz and real-time capability. A system which covers

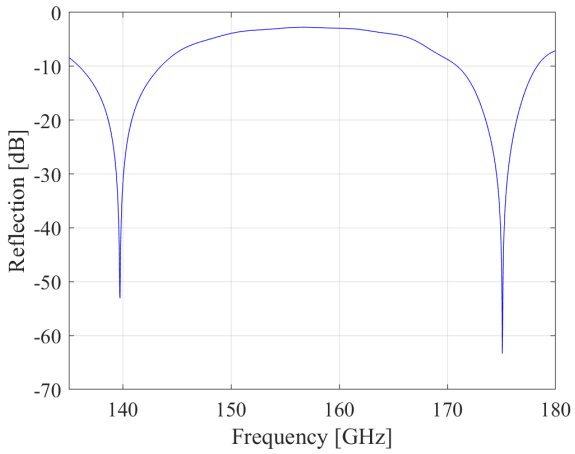

Fig. 7: Reflection measurement result of a CVD-diamond disk.

all of the requirements is extremely expensive. Therefore, different solutions are proposed using different technologies to satisfy the requirements. The initial frequency diagnostic systems are limited to 175 GHz, however, future applications call for frequencies up to 240 GHz. Therefore, the current frequency diagnostic systems have been upgraded, which is discussed in the following sections.

4.1 Frequency Measurement System (FMS)

The electromagnetic wave couples out through the relief window of the gyrotron. The wave is guided to the FMS for evaluation via a waveguide that is several meters long. This relief window is positioned off-axis. It allows to couple out the stray radiation of the mirror box of the gyrotron. Depending on the electromagnetic field inside mirror box, the stray radiation level can be different. It is not possible to predict the maximum power level at FMS. For safety reasons, several variable attenuators with a maximum attenuation of 40 dB each are installed in front of the subharmonic mixers. That mixers allow a maximum input power of +10 dBm. In addition, an isolator is installed in front of the down-mixing stage to prevent reflected signals from propagating back to the gyrotron. A schematic view of the upgraded real-time capable FMS system is shown in Fig. 8. The existing system consists of only one mixer covering a frequency bandwidth of only 110-175 GHz. For the upgraded system, the FMS should continuously operate from 110-260 GHz, which covers two waveguide frequency bands. Therefore, the down-conversion is separated into two paths from 110-170 GHz and 170-260 GHz, as depicted in Fig. 8. The required frequency band is chosen by the operator using electronically controlled attenuators. The new mixers are sub-harmonic mixers operating at the second harmonic, which reduces the conversion losses compared to mixers operating at higher harmonics and thus resulting in a higher dynamic range. The intermediate frequency (IF) bandwidth of the mixers is 18 GHz. The IF signals are amplified and divided by a power divider into two different paths, one evaluated by a filterbank [20] and the second by a Modulation Domain Analyzer.

4.1.1 Filterbank

The filterbank divides the 18 GHz input spectrum into 9 adjacent sub-channels with 2 GHz bandwidth each. Afterwards, diodes produce DC voltages, which are proportional to the input RF power of the individual channel and are displayed on an oscilloscope. A signal on the display of an individual channel indicates that a mode in the corresponding frequency band is being excited. This setup is used to have a fast overview of the excited modes. The filterbank has a very large evaluating real-time bandwidth of 18 GHz, but suffers

from a frequency resolution of only 2 GHz. However, a resolution of 2 GHz is sufficient for this study, because the frequency separation of the neighboring modes is 2.1 GHz and thus, each of the 9 channels corresponds to a specific mode. The calculated dynamic range of the filterbank diagnostic system is 24 dB.

4.1.2 Modulation-Domain Analyzer (MDA)

The second evaluation method of the FMS system uses an HP MDA to detect the transient response in a given frequency band. The bandwidth of the MDA is specified to be 2.5 GHz, which implies that a more precise measurement of one of the 9 filterbank channels can be performed. Therefore, a further mixer stage with a low-pass filter is used to convert the IF signal into the desired frequency band below 2.5 GHz. The MDA has a minimum frequency resolution of 100 kHz and an improved dynamic range from initial 20 dB to 23 dB with the upgraded system.

4.2 Pulse Spectrum Analysis (PSA) System

The disadvantages of the FMS system are a trade-off between frequency resolution and bandwidth, possible mixing effects (ambiguity of mixers) and a low dynamic range. Therefore, an alternative diagnostic has been developed in [19]. The goal of the PSA system was: (i) unambiguous reconstruction of the RF spectrum from the IF signals, (ii) high dynamic range for parasitic oscillation detection, (iii) high bandwidth for mode competition investigation (e.g. mode switching), (iv) high frequency resolution for the diagnosis of frequency instabilities or modulation and (v) detection of transient behavior. However, the real-time capability is not given, because a post-processing of the data is required.

The schematic view of the PSA system is shown in Fig. 9a. The mixers have an IF bandwidth of $\Delta f_{\mathrm{IF}} = 3.5$ GHz each. An unambiguous down-conversion can be performed with 2 channels, each equipped with a mixer to which different local oscillator (LO) frequencies are applied. In addition, the operating harmonic of the mixers are different to reduce false positives, as can be seen in Fig. 10. The signals in the IF-band are sampled using an oscilloscope. The sampled signals are transformed from the time domain to the frequency

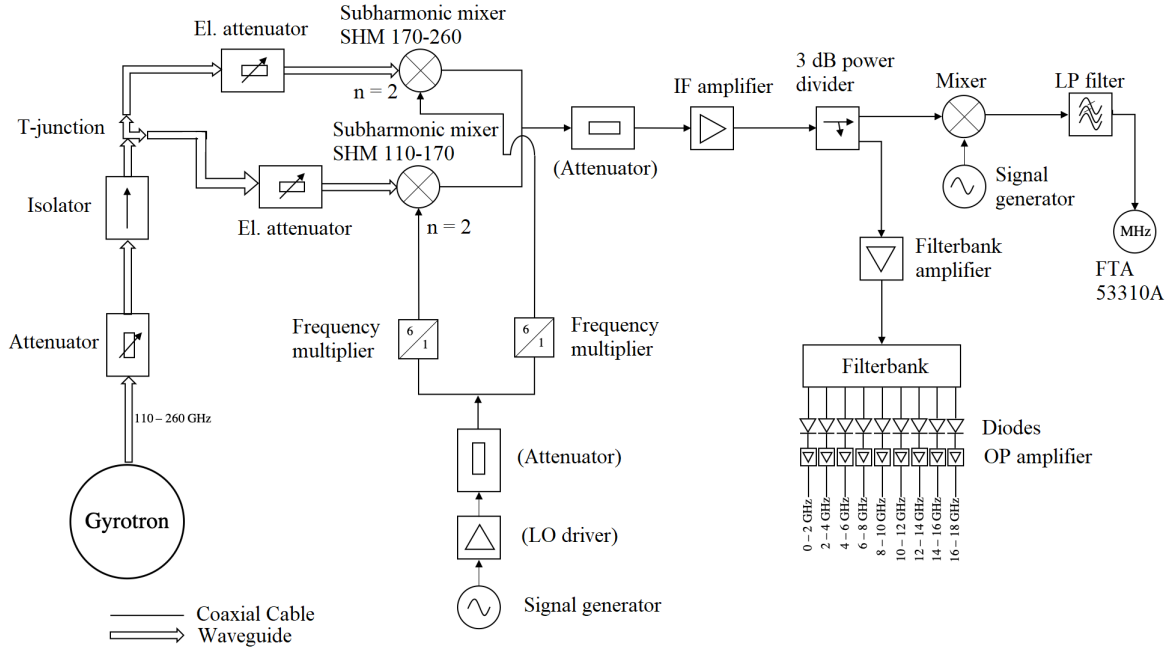

Fig. 8: Schematic of the modified FMS system covering a frequency bandwidth from 110-260 GHz.

domain using a short-time frequency transformation. The reconstruction is done in the post-processing using a minimum search on numerically shifted and mirrored terms of the spectra $S_1(f, t_i)$ of channel 1 and $S_2(f \pm f_d, t_i)$ of channel 2, where f_d is the difference of the LO frequencies. The high R_{HSI} and low side band reconstructed RF spectrum R_{LSI} is calculated with [19]:

$$R_{\mathrm{LSI}} = \mathrm{Min}(S_1(f, t_i), S_2(f - \Delta f_d, t_i)) \qquad \forall i \tag{4}$$

$$R_{\mathrm{HSI}} = \mathrm{Min}(S_1^{\leftrightarrow}(f - \Delta f_d, t_i), S_2^{\leftrightarrow}(f, t_i)) \quad \forall i \tag{5}$$

The IF spectrum calculation between 0 and Δf_D is not included in the formulas mentioned before. This remaining part of the spectrum R_{x} can be reconstructed using:

$$R_{\mathrm{x}} = \mathrm{Min}(S_1^{\leftrightarrow}(f + \Delta f_d, t_i), S_2(f, t_i)) \quad \forall i \tag{6}$$

The combination of R_{HSI}, R_{x} and R_{LSI} forms the fully reconstructed spectrum. The effective bandwidth of the reconstructed RF spectrum is $2 \cdot \Delta f_{\mathrm{IF}} - \Delta f_d$. In practice the effective bandwidth is 6 GHz per channel pair. In the implementation two independent channel pairs are build, where the effective bandwidth is increased to 12 GHz. As a result, a spectrogram can be produced. A spectrogram shows the frequency spectrum over time where the transient behavior can be investigated. There is always a trade-off between frequency resolution δf and time resolution in the spectrogram, defined by the time segment T_{seg}, which is inverse proportional to each other $\delta f = 1/T_{\mathrm{seg}}$. A common used frequency resolution of the PSA is 1 MHz. The acquisition time is limited to 14 ms (one channel pair) and 7 ms (two channel pairs) at the maximum sampling rate. The calculated dynamic range is given by 60 dB [19]. An example of a spectrogram is shown in Fig. 9b. It shows the start-up of the gyrotron during which the frequency is tuned to the nominal operation frequency reaching flat-top of the power supplies at 260 µs. At 320 µs, another oscillation is generated and competes with the nominal mode where a strong modulation occurs. This competing mode becomes dominant from 355 µs, where a mode switch takes place. The gyrotron pulse ends at 370 µs.

The current PSA system can easily be upgraded from its limit at 175 GHz, by replacing the mixers. The most important part is the choice of the harmonic $h_{n,d}$ of the mixer 1 $h_{1,d}$ and of mixer 2 $h_{2,d}$ to reduce false positives. A calculation is shown in Fig. 10. It is obvious, that mixers working on similar harmonics have the highest number of false positives. Therefore, the harmonics of the mixers in a channel pair are not equal. A prime number end up with the lowest number of false positives. However, these mixers are custom made products and are expensive. The mixers on the market that operate in the frequency range of 170-260 GHz typically operate at harmonics $h = 14$, 16 or 18. Regarding Fig. 10, all of these combinations lead to two false positives. A combination of 14 and 16 has been chosen, because a lower harmonic leads to lower conversion losses. The assembly and test of all of the components will be performed in mid of 2021.

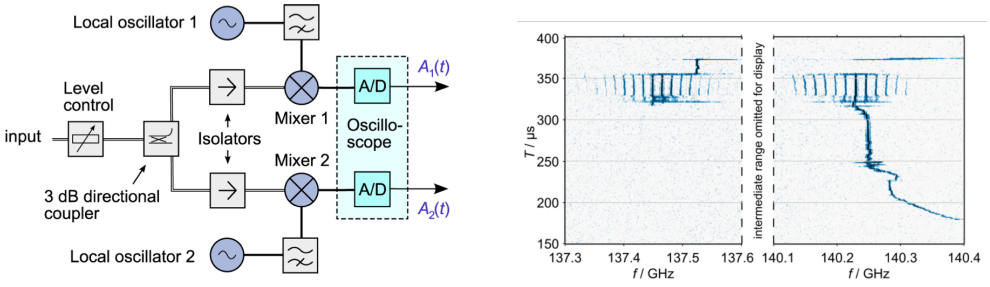

(a) Schematic of PSA. **(b)** Spectrogram.

Fig. 9: (a) Schematic view of one channel pair and (b) example of a spectrogram using the PSA system [19].

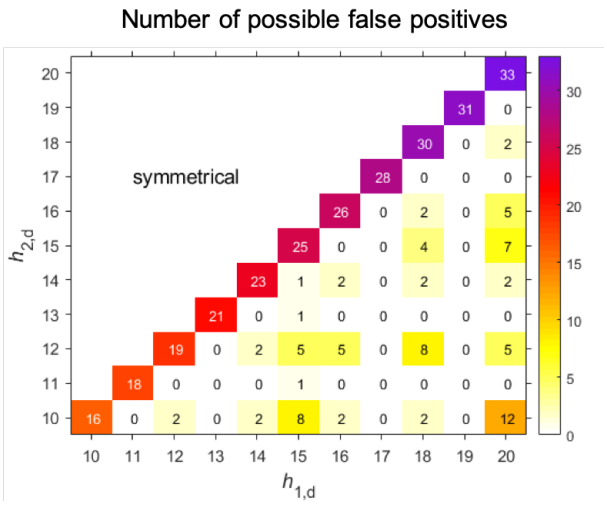

Fig. 10: Calculated false positives in the frequency band from 170-260 GHz according to the mixer harmonics h of mixer 1 $h_{1,d}$ and mixer 2 $h_{2,d}$.

5 Conclusion

Different mm-wave measurement setups for MW-class gyrotrons are discussed for cold and hot measurements. All of the relevant frequency dependent measurement systems have been upgraded for R&D of DEMO relevant gyrotrons operating above 200 GHz. The verification of the quasi-optical output system is upgraded with frequency extension modules to cover a frequency bandwidth from 90-330 GHz. In addition, high-precision linear-drivers are installed to achieve higher position accuracy and thus excite rotating high-order gyrotron modes with a high purity. As an example, the excitation of the $TE_{40,23}$ mode operating at 204.074 GHz and the verification of a quasi-optical output system at 140 GHz is presented. The window measurement teststand includes the verification of the CVD-diamond gyrotron output window. This measurement system is equipped with the similar frequency extension modules mentioned before, where a frequency bandwidth from 90-330 GHz is covered. In addition, in hot measurements the frequency diagnostic systems of the gyrotron are important. At IHM/KIT, two independent frequency diagnostic systems, namely FMS and PSA, have been developed in the past. They have been upgraded from their limit at 175 GHz to measurement setups in the range of 110-260 GHz. Sub-harmonic mixers, working at the second harmonic, are considered for the FMS system, where an increase of the dynamic range of 3 dB is achieved. The desired frequency band (110-170 GHz or 170-260 GHz) can be chosen by electronically controlled attenuators. The observing frequency range is given by the IF range of 18 GHz. The second system, the PSA, will be equipped with two additional channel pairs to cover the frequency band from 110-260 GHz. Calculations have been performed to determine the combination of the mixer harmonics having the lowest possible number of false positives. This setup is planned to be build up in 2021.

Funding: This work has been partly carried out within the framework of the EUROfusion Consortium and has been received funding from the Euratom research and training programme 2014-2018 and 2019-2020 under grant agreement No. 633053. The views and opinions expressed herein do not necessarily reflect those of the European Comission. Part of the simulations were performed on the EUROfusion High Performance Computer (Marconi-Fusion).

References

[1] T. Rzesnicki et al., 2.2-MW record power of the 170-GHz European pre-prototype coaxial-cavity gyrotron for ITER, IEEE Transactions on Plasma Science, Vol. 38, No. 6, pp. 1141-1149, 2010.

[2] G. Gantenbein et al., New trends of gyrotron development at KIT: An overview on recent investigations, Fusion Engineering and Design, Vol. 146, pp. 341-344, 2019, doi:10.1016/j.fusengdes.2018.12.063.

[3] R. C. Wolf et al., Electron-cyclotron-resonance heating in Wendelstein 7-X: A versatile heating and current-drive method and a tool for in-depth physics studies. Plasma Physics and Controlled Fusion, **61**, 2019.

[4] H. Zohm et al., On the use of step-tuneable gyrotrons in ITER, Journal of Physics: Conference Series 25 (2005) 274-282. doi:10.1088/1742-6596/25/1/033.

[5] J. Stober et al., ECRH on ASDEX Upgrade - System status, feed-back control, plasma physics results, EPJ Web of Conferences 32, 02011, (2012), doi:10.1051/epjconf/20123202011.

[6] R. Wolf et al., Major results from the first plasma campaign of the Wendelstein 7-X stellarator, Nuclear Fusion, 57, 102020, (2017).

[7] C. Darbos et al. Status of the ITER EC system, in: Proc. IEEE PPS, San Francisco, USA, 2013, pp. P5-P22.

[8] G. Frederici et al. Overview of EU DEMO design and R&D activities, Fusion Engineering and Design (2014), pp. 882-889.

[9] M. Schmid et al. The 10MW EPSM modulator and other key components for the KIT gyrotron test facility FULGOR. Fusion Engineering and Design, 123:485-489, 2017. Proceedings of the 29th Symposium on Fusion Technology (SOFT-29), Prague, Czech Republic, September 5-9, 2016.

[10] H. U. Nickel and T. Geist, Diagnostic and instrumentation for millimetre-wave gyrotrons, Gyrotron Oscillators: Their Principles and Practice by C. J. Edgecombe, Cambridge University Press, Chapter 13, 1993.

[11] K. Avramidis et al., Towards a 1.5 MW, 140 GHz gyrotron for the upgraded ECRH system at W7-X, 31st Symposium on Fusion Technology (SOFT 2020)

[12] N. L. Alexandrov et al., Low-power excitation of gyrotron-type modes in a cylindrical waveguide using quasi-optical techniques, International Journal of Electronics, 79, pp. 215-216, (1995).

[13] D. Wagner, J. Pretterebner, M. Thumm, Design of coaxial gyrotron cavities using a scattering matrix code, 5th Joint Russian-German Meeting on ECRH and Gyrotron, pp. 555-565, (1993).

[14] T. Ruess et al., Computer-controlled test system for the excitation of very high-order modes in highly oversized waveguides, Journal of Infrared, Millimeter,and Terahertz Wave 40, 257-268, (2019), doi:10.1007/s10762-018-0566-3.

[15] J. Jin, M. Thumm, B. Piosczyk, et al.. Novel numerical method for the analysis and synthesis of the fields in highly oversized waveguide mode converters, IEEE Transactions on Microwave Theory and Techniques, 57, 1661-1668 (2009).

[16] M. Thumm: State-of-the-art of high-power gyro-devices and free electron maser,. Journal of Infrared, Millimeter, and Terahertz Waves, 41, No. 1, 1-140 (2020), doi.org/ 10.1007/s10762-019-00631-y.

[17] H.-U. Nickel and M. Thumm: Plane transverse waveguide windows - survey of formular for reflection, transmission and absorption, Conference Digest, 16th International Conference on Infrared and Millimeter Waves, Lausanne, 1991, Proc., SPIE 1576, pp. 444-445.

[18] H. O. Prinz, Frequency measurement system for gyrotron diagnostics, in IEEE Potentials, vol. 26, no. 4, pp. 25-30, July-Aug. 2007, doi:10.1109/MP.2007.4280329.

[19] A. Schlaich et al., Transient millimeter-wave signal analysis with unambiguous RF spectrum reconstruction, in IEEE Transactions on Microwave Theory and Techniques, vol. 61, no. 12, pp. 4660-4666, Dec. 2013, doi: 10.1109/TMTT.2013.2283063.

[20] T. Geist, M. Thumm and W. Wiesbeck: Contiguous filterbank receiver for a pulsed 140 GHz gyrotron, Conference Digest, 16th International Conference on Infrared and Millimeter Waves, Lausanne, 1991, Proc., SPIE 1567, pp. 274-275.